ORIGINAL RESEARCH **Open access**

A Robust AI-Driven Hybrid Approach for Power System Flicker Component Identification

Lucia Romano[1*], Marco Bellini[2], Paolo Greco[1]

Abstract

This paper proposes an innovative hybrid technique that integrates H-∞ filtering together with an adaptive linear neuron (ADALINE) network to estimate flicker components within power distribution networks. The developed approach takes advantage of the H-∞ filter's strong robustness to obtain the voltage envelope in uncertain and noisy settings, after which ADALINE is applied to determine the relative amplitudes of flicker components (ΔVi / Vt) at the IEC-specified frequencies contained in the envelope. This integration supports effective time-domain estimation, featuring quick convergence and excellent noise resistance, resolving significant shortcomings of conventional frequency-domain strategies. Unlike standard procedures, the hybrid model effectively handles complex power disturbances without requiring detailed knowledge of noise properties or large-scale training. Performance validation involved simulation experiments aligned with IEC Standard 61000-4-15, complemented by statistical assessments, Monte Carlo trials, and practical field measurements. Findings reveal greater precision, greater durability, and lower processing requirements compared with Fast Fourier Transform (FFT) and Discrete Wavelet Transform (DWT)-based estimation methods.

Keywords Flicker, Voltage fluctuations, Estimation process, H-infinity, Adaptive linear neuron, Neural network

*Correspondence:
Lucia Romano
lucia.romano@uniroma1.it
[1] Department of Smart Energy Intelligence, Faculty of Engineering, Sapienza University of Rome, Rome, Italy
[2] Department of AI and Power System Optimization, Faculty of Engineering, Polytechnic University of Milan, Milan, Italy

Introduction

Voltage fluctuation indicates a succession of changes or persistent variations in the root-mean-square (RMS) or peak value of the voltage. Per power quality standards, the size of these variations usually remains below 10% of the nominal voltage [1, 2]. Voltage fluctuations often result in light flicker, recognized as irregular brightness or changes in the spectral composition of light sources. Such problems are particularly important in renewable energy systems, as the inconsistent output from wind and solar sources often causes dynamic, unexpected voltage shifts that trigger flicker [3, 4]. It should be noted that while voltage fluctuations are the chief source of flicker in power systems, the visibility of flicker also depends significantly on the properties of the lighting equipment. Incandescent lamps, because of their thermal inertia, dampen high-frequency voltage fluctuations. In contrast, fluorescent and LED lamps — mainly those fitted with inferior driver circuits — might transform even minor disruptions into perceptible brightness changes [5, 6].

Additionally, embedded electronic buffers or power-factor correction features in current lamps can increase or decrease flicker sensitivity. Therefore, voltage fluctuations constitute a necessary yet insufficient condition for light flicker; the overall outcome stems from the interplay among the electrical disturbance, lamp behavior, and human visual perception, as outlined in the IEC 61000-4-15 standard. To measure this flicker, the IEC flicker meter accounts for the human eye-

This is an open access article distributed under the terms of the Creative Commons Attribution-NonCommercial-ShareAlike 4.0 International License (CC BY-NC-SA 4.0), which permits non-commercial use, distribution, reproduction, and adaptation in any medium or format, provided that appropriate credit is given to the original author(s) and source, a link to the license is provided, and any changes made are indicated. Adapted material must be distributed under the same license.

© 2022 The Author(s). | Published by Institute of Smart Energy Systems Press

brain response to light changes. The main result from the IEC flicker meter is the instantaneous flicker sensation (S). The IEC 61000-4-15 standard establishes four analytical stages to determine flicker sensation [5, 7-9]. The initial stage normalizes the incoming voltage waveform against an internal reference. In the second stage, the output undergoes squaring. Block 3 applies demodulation filters afterward, including a high-pass filter (cut-off at 0.05 Hz), a low-pass filter (cut-off at 35 Hz), and a weighting filter. Lastly, Block 4 derives the S parameter by squaring the signal and dividing by the average to standardize the results.

Although the IEC procedure requires ongoing voltage input to compute flicker, the filtering stage imposes a significant computational burden in practice. Hence, multiple substitute techniques utilizing discretized waveforms have emerged. A substantial number of these are based on the discrete Fourier transform (DFT), representing a frequency-domain method [10-12]. Yet, DFT-based techniques encounter issues such as aliasing, picket-fence effects, and leakage phenomena, each of which can significantly reduce accuracy in the presence of noise and disturbances [13]. To reduce these difficulties, some investigators have recommended frequency-domain strategies that employ the Z-transform to correct leakage errors [14, 15]. In addition to Z-transform strategies, sophisticated methods such as Dynamic Voltage Restorers (DVRs) combined with Multi-Level Inverters (MLIs) have been deployed to mitigate voltage sags, swells, and flickers. Innovative designs, for instance, a 33-level Asymmetrical MLI, strengthen Low and High Voltage Ride Through (LVRT, HVRT) features, displaying better results in addressing flicker and harmonic problems [16]. Even with reasonable performance in specific situations, these approaches continue to exhibit reduced accuracy when noise and harmonics are present.

To tackle these restrictions, merging the Z-transform with the Teager energy operator has been proposed [17, 18], delivering superior accuracy at elevated sampling rates but increasing computational demands. Besides this, such techniques commonly limit themselves to a narrow selection of harmonics and flicker elements within simulations. In light of the weaknesses of frequency-domain processors, substantial research has focused on time-domain processing approaches [19, 20], which are commonly used to estimate harmonic components in power systems [21-24]. Because flicker elements appear as frequency elements adjacent to the fundamental frequency, the selected methods require robustness to interactions with nearby frequencies to recognize flicker components correctly.

In Saleh [25], Saleh [26], Sun *et al*. [27], and Kuwalek [28], amplitude modulation (AM) is analyzed for its potential to estimate flicker components in distributed generation (DG) systems using several filters. Though this method is simple, its accuracy depends heavily on the number of filters applied, and actual deployments may encounter barriers due to increased processing time when full flicker waveforms are required. Analytical reviews of flicker meter effectiveness based on IEC 61000-4-15 appear in Yang and Kratz [29], Geiger and Halpin [30], Balouji and Salor [31], and Cho *et al*. [32]. These examinations use RMS voltage inputs in offline mode, which suits planning activities but is limited for real-time operations. Despite confirmation of outcomes through simulations and on-site testing, flicker meters typically deliver accurate results for low-frequency inputs but are inconsistent for higher-frequency variations [30].

Artificial neural networks (ANNs) serve as robust tools for optimization and estimation and have been deployed for flicker identification in power systems [33, 34]. Nevertheless, the number of network inputs often increases when ANNs are directly applied to flicker index retrieval, thereby increasing computational complexity. To counter this, multi-stage networks featuring pre-processing layers have been formulated [35]. While these strategies deliver adequate performance in certain instances, they remain largely restricted to offline use.

The Kalman filter (KF), along with its variants, has gained broad acceptance as an essential tool for investigating and resolving multiple estimation problems [26, 27]. Various researchers have implemented state-variable models of nonlinear flicker waveforms to estimate flicker components using diverse KF types [36-39]. Although KF-based strategies deliver reliable results when focusing on a constrained set of flicker frequencies, their precision declines as the frequency span widens. Moreover, elementary KF algorithms remain vulnerable to instability whenever noise and variations appear in the reference signal.

© 2022 The Author(s). | Published by Institute of Smart Energy Systems Press

In this paper, we introduce a novel time-domain hybrid approach, the Hybrid Envelope Flicker System (HEFS), for determining flicker components from modulated voltage signals in power systems [40]. The algorithm proceeds in two distinct phases: initially, a robust H-∞ filter estimates the waveform envelope [41]; afterward, an online neural network (e.g., ADALINE) computes the flicker components [42-44]. This technique stands out for its straightforward framework and reliable functionality. The core contributions from this research are outlined here:

Although numerous studies exist on flicker estimation, most techniques struggle to maintain reliable performance amid non-sinusoidal interference from harmonics, noise, and complex modulation that alter voltage signals. Modern ANN-based systems typically require extensive input dimensions and massive training datasets, whereas Kalman filters often falter when faced with model uncertainty or strict assumptions. Such shortcomings prompted the design of an approach that combines robustness to uncertainty with strong efficiency for real-time deployment. This research focuses specifically on interferences caused by voltage flicker, harmonic distortion, and additive white noise — elements that often appear simultaneously in actual power networks. The primary contributions of this paper appear below:

1. Applies a robust H-∞ estimator with a clear, simple structure that successfully detects flicker in modulated voltage waveforms despite unknown noise interference.

2. Makes use of the ADALINE neural network [45], offering swift estimation that processes several envelopes without any prior training period and supplies an effective solution for assessing voltage changes when power harmonics are present.

3. Presents an innovative voltage variation framework incorporating both harmonic and flicker elements to deliver a truer depiction of real power signals.

4. Pulls out various flicker frequencies from changing voltage waveforms while capturing every key frequency element specified in the IEC 61000-4-15 standard.

5. Suggests a combined algorithm that distinguishes carrier frequencies from flicker frequencies of unequal amplitudes, delivering speedy convergence independent of usual filtering techniques.

Overall, combining H-∞ filtering with ADALINE yields a unique two-phase strategy that enables precise real-time assessment of harmonic and flicker components while meeting IEC 61000-4-15 requirements.

Materials and Methods

According to the IEC standard, voltage waveforms containing flicker components are modeled as an amplitude-modulated (AM) signal. Here, the power system frequency (50 or 60 Hz) operates as the carrier, with the flicker frequency (envelope) acting as the message. This link receives expression in discrete format [2]:

$$Z^k = V_c \cos(2\pi f k\tau_s)\left\{1 + \sum_{i=1}^{F} \frac{\Delta V_i}{2V} \cos(2\pi F_i k\tau_s + \theta_i)\right\} \quad (1)$$

Where Vc stands for the carrier amplitude (nominal voltage amplitude), f indicates the power system frequency, and the index i = 1, 2, …, F points to every flicker component. Fi and θi denote the frequency and phase angle belonging to the ith flicker component, while $\frac{\Delta V_i}{2V}$ denotes the relative voltage fluctuation. Implementation of the model in discrete form relies on the sampling period τs. The proposed algorithm seeks to determine the relative voltage amplitude $\frac{\Delta V_i}{2V}$ belonging to each flicker component. Note that across all equations, the superscript k indicates the discrete time instant.

© 2022 The Author(s). | Published by Institute of Smart Energy Systems Press

Nonlinear loads distort power system voltage waveforms. The former model given in **Eq. 1** fails to capture the complexities of actual power signals. For this reason, the current paper proposes a new voltage variation model that accounts for harmonic and flicker components simultaneously. Furthermore, accurate noise representation incorporates an added high-frequency noise term into the signal model:

$$Z^k = \sum_{n=1}^{N} V_n \cos(2\pi n f k\tau_s + \phi_n)\left\{1 + \sum_{i=1}^{F} \frac{\Delta V_i}{2V_t}\cos(2\pi F_i k\tau_s + \theta_i)\right\} + \sigma \cdot \mathrm{randn}_k \quad (2)$$

Where n= 1, 2, …, N indicates harmonic order. Vn gives the amplitude for each harmonic, while ϕn gives its phase. represents Gaussian noise with standard deviation σ, setting the noise power level. The value $V_t = \sqrt{\sum_{n=1}^{N} V_n^2}$ functions as the base for normalizing voltage fluctuations.

Because the model has many states with wide-ranging amplitudes, hybrid algorithms improve flicker estimation. The suggested hybrid algorithm runs across two sequential phases. At the start, the H-∞ filter extracts the envelope from the varying voltage waveform during every time step k. This extracted envelope then moves to the ADALINE network, enabling calculation $\frac{\Delta V_i}{V_t}$ of the values tied to each frequency at the given instant.

Envelope estimation using the H-∞ method

As a popular analytical estimator, the H-∞ filter aims to reduce the worst-case estimation error [46]. It effectively handles time-varying signal estimation even in the presence of unknown noise, setting it apart from KF-based techniques that focus on reducing the expected error variance. Estimation of envelopes via the H-∞ filter begins by reformulating the modulated signal from **Eq. 2** in this manner:

$$Z^k = A_1\{\mathrm{Envelope}_1\} + A_2\{\mathrm{Envelope}_2\} + \cdots + A_N\{\mathrm{Envelope}_N\} + \sigma \cdot \mathrm{randn}^k \quad (3)$$

where:

$$\mathrm{Envelope}_n = V_n + \sum_{i=1}^{F} \frac{V_n \Delta V_i}{2V_t}\cos(2\pi F_i k\tau_s + \theta_i) \quad (4)$$

Power frequency components A_n = cos ($2\pi nfk\tau_s + \phi_n$) undergo expansion through trigonometric identities:

$$A_n = \cos(2\pi n f k\tau_s)\cos(\phi_n) - \sin(2\pi n f k\tau_s)\sin(\phi_n) \quad (5)$$

A Phase-Locked Loop (PLL) sourced from the MATLAB toolbox helps maintain the actual power frequency, which is especially useful amid challenges with frequency deviation. Drawing from **Eq. 3** yields a linear model designed for the H-∞ estimator:

$$Z^k = H^k x + \omega^k \quad (6)$$

© 2022 The Author(s). | Published by Institute of Smart Energy Systems Press

where ωk forms the measurement noise matrix and the state vector x receives definition as:

$$x = [\cos(\phi_1)\text{Envelope}_1 \sin(\phi_1)\text{Envelope}_1 \ldots \cos(\phi_N)\text{Envelope}_N \sin(\phi_N)\text{Envelope}_N] \quad (7)$$

Envelope details reside inside the state vector x. The structure matrix Hk takes the form:

$$H^k = [\cos(2\pi f k\tau_s) - \sin(2\pi f k\tau_s) \ldots \cos(2\pi N f k\tau_s) - \sin(2\pi N f k\tau_s)] \quad (8)$$

Measurement Z^k allows time-domain estimation of the state vector x according to the time-update equation:

$$\hat{x}^k = \Phi(\hat{x}^{k-1} + K^k(Z^k - H^k\hat{x}^{k-1})) \quad (9)$$

Where K^k and Φ serve as the gain and state transition matrices, with unknown time-varying state behavior, Φ takes the form of a fixed identity matrix. Recursive updates apply to the estimation error covariance matrix through reduction of the worst-case estimation error:

$$P^k = \Phi P^{k-1}(I - \alpha P^{k-1} + H^{kT} R^{-1} H^k P^{k-1})^{-1}\Phi^T \quad (10)$$

Where factor α manages the effect of prior errors during estimation and receives selection by the filter designer according to the problem. R stands for the measurement noise covariance matrix. Computation of the gain matrix K^k relies on the estimation error covariance matrix:

$$K^k = P^k(I - \alpha P^k + H^{kT} R^{-1} H^k P^k)^{-1} H^{kT} R^{-1} \quad (11)$$

Envelopes become available at every time step k from state information:

$$\text{Envelope}_1 = \sqrt{x_1^2 + x_2^2}, \ldots, \text{Envelope}_n = \sqrt{x_{N-1}^2 + x_N^2} \quad (12)$$

In essence, the H-∞ functions as a sturdy state estimator focused on cutting worst-case estimation error amid all possible disturbances — unlike the Kalman filter's emphasis on expected error covariance. The optimization target maintains the ratio of estimation error energy to disturbance energy under a defined threshold γ:

$$\frac{\|e_k\|_2^2}{\|\omega_k\|_2^2} < \gamma^2 \quad (13)$$

Where ek marks the estimation error and ωk the measurement noise, such a design builds resilience when noise statistics remain unknown. Practically speaking, the filter continuously updates state estimates using measurement innovations while limiting disturbance amplification. Solving the optimization involves calculating the gain matrix Kk (as shown earlier)

© 2022 The Author(s). | Published by Institute of Smart Energy Systems Press

to support convergence in the presence of uncertainty and noise. Consequently, the H-∞ framework fits power quality estimation tasks particularly well, as voltage signals often contain unmodeled disturbances and random noise.

With its straightforward steps and modest computational requirements, the H-∞ estimator is well-suited to real-world applications. Estimated envelopes feed into the ADALINE network at each step for flicker component calculation. Further details on this appear in the next subsection.

Flicker components estimation using ADALINE

Time-varying amplitude envelopes are obtained via **Eq. 12** at each time step. These then enter an online ADALINE neural network intended for spectral analysis. ADALINE delivers value through its basic architecture, which skips a training phase, making it well-suited for quick estimation tasks. The algorithm further benefits from requiring only a few adjustable parameters, easing practical use. **Figure 1** displays the ADALINE network schematic. Target states involve flicker amplitudes at frequencies inside the range $f \pm Fi$ Hz, with f as the power frequency and Fi drawn from IEC standard 61000-4-15 details in **Table 1.**

Flicker amplitude estimation models the H-∞ filter's extracted envelope using flicker frequencies taken from **Table 1**. The network has 74 inputs representing DC values.

Table 1. Flicker frequencies Fi in Hz based on IEC standard 61000-4-15.

Flicker frequencies F_i (Hz)					
0.5	3.5	6.5	10	14	20
1	4	7	10.5	15	21
1.5	4.5	7.5	11	16	22
2	5	8	11.5	17	23
2.5	5.5	8.8	12	18	24
3	6	9.5	13	19	25

The selection of the 74 frequencies listed in **Table 1** follows the IEC Standard 61000-4-15 guidelines for the flicker frequency span (0.5–25 Hz), which is most closely tied to human visual sensitivity. They establish a static grid of basis functions, enabling the ADALINE network to estimate flicker amplitudes efficiently. Despite its discrete character, the algorithm's adaptive quality supports approximation of off-grid elements via leakage into neighboring frequencies. This creates a sensible trade-off among resolution, ease of computation, and avoidance of constant reconfiguration.

$$x_{ad}^{k} = [1, 0, \cos(2\pi 0.5 k\tau_s) - \sin(2\pi 0.5 k\tau_s) \ldots \cos(2\pi 25 k\tau_s) - \sin(2\pi 25 k\tau_s)]^T \quad (14)$$

For the nth envelope at time step k the weight vector equals:

$$w_n^k = [w_{1n}^k, w_{2n}^k, \ldots, w_{73n}^k, w_{74n}^k] \quad (15)$$

Weight updates follow the Widrow–Hoff rule:

© 2022 The Author(s). | Published by Institute of Smart Energy Systems Press

$$w_n^{k+1} = w_n^k + \frac{\theta^k e_n^k x_{ad}^{k^T}}{\lambda + x_{ad}^{k^T} x_{ad}^k} \quad (16)$$

Where e_n^k marks the tracking error, and λ prevents division by zero. Calculation of the adaptive learning factor θ^k proceeds as:

$$\theta^k = \frac{\theta^0}{1 + \frac{k}{\beta}} \quad (17)$$

Within **Eq. 17,** the constant β sets the decay speed for the starting learning rate θ0. Final weights in this setup hold the flicker data. Extraction of harmonic and flicker amplitudes uses this expression:

$$V_n = \sqrt{w_{1n}^2 + w_{2n}^2} \quad \text{and} \quad \frac{\Delta V_i}{2V_1} = \frac{\sqrt{w_{(2i+1)n}^2 + w_{(2i+2)n}^2}}{V_n}, \quad i = 1, 2, \ldots, F \quad (18)$$

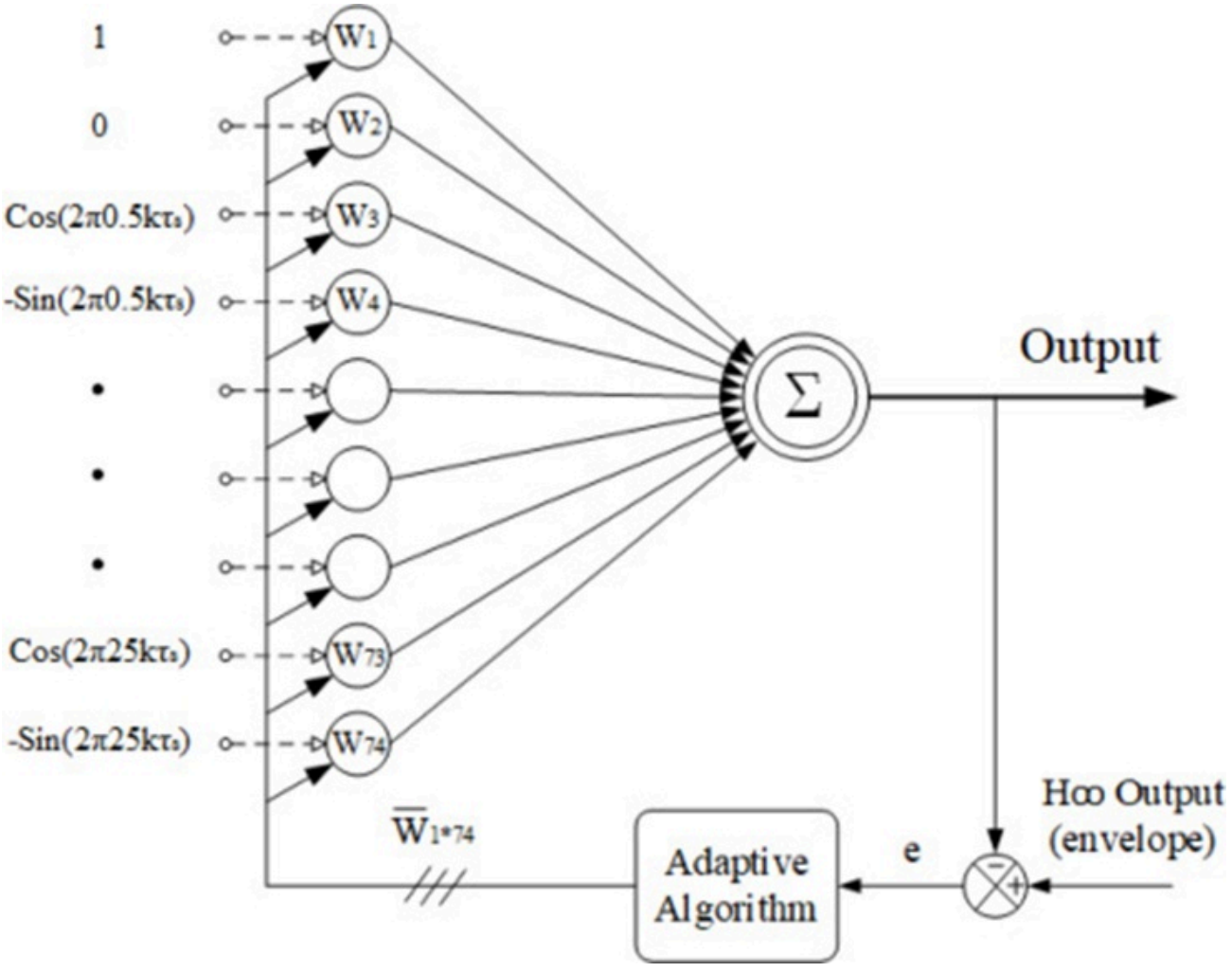

Figure 1. Block diagram of the ADALINE neural network used for flicker frequency estimation. The input consists of sinusoidal basis functions covering a predefined flicker frequency range. Each input is weighted by a corresponding

© 2022 The Author(s). | Published by Institute of Smart Energy Systems Press

coefficient Wi, and the weighted sum forms the ADALINE output. The output is compared against the reference envelope obtained from the H-∞ filter. The resulting error e is used in the Least Mean Squares (LMS) adaptive algorithm to update the weights in real time, minimizing the squared error and allowing the network to track multiple flicker components. ADALINE network final outputs consist of relative flicker amplitudes $\Delta Vi/Vt$ aligned with standard flicker frequencies Fi. These correspond to the physical flicker measures outlined in IEC 61000-4-15 and support direct computation of instantaneous flicker sensation (S) plus additional standard indices. Hence, the suggested method goes beyond mere frequency tracking by directly determining the relative amplitudes of flicker components, which carry clear physical and perceptual meaning.

Results and Discussion

Several simulations were run to evaluate the performance of the proposed approach for determining flicker components. These tests relied on the waveform model given in **Eq. 2**. The frequency composition of this waveform corresponds to the voltage at industrial load buses, which commonly features harmonics ranging from the 1st to the 11th. Significant flicker elements drawn from IEC Standard 61000-4-15 were also integrated into the waveform. To showcase the durability of the suggested technique, the flicker estimation task was performed on a heavily distorted signal containing five harmonics and superimposed high-frequency noise.

Suitable parameter selections were made for the suggested technique. The adopted settings for the H-∞ filter and the ADALINE neural network are displayed in **Table 2.**

I indicates the identity matrix, and 1 denotes a vector consisting of ones. These chosen parameters were kept unchanged for the entire set of simulations. The core software simulations reviewed in this work are outlined here:

Table 2. Parameters for H-∞ filter — ADALINE neural network simulations.

H_∞ method		ADALINE method		Simulation	
P^0	$10^3 \cdot I^*_{2N\times 2N}$	w^0	1^{**}_{2i+2}	τ_s	1/1200
$\hat{x}_0$	1^{**}_{2N}	θ_0	5	σ	0.02
α	8	λ	0.0001		
f	50	β	1000		
R	0.007				

1. Simulated waveform with one power harmonic and one flicker component.

2. Distorted waveform with 5 power harmonics and 36 flicker components. This test evaluates the suggested method's ability to track flicker in the presence of multiple harmonics.

3. Monte Carlo (MC) simulation for analyzing the suggested method. This test demonstrates the method's generalization capability, since the harmonics and flicker amplitudes are randomly selected in the signal model.

Estimation of a waveform with power frequency and one flicker component

In a representative example, a waveform was generated that included the fundamental power frequency and a single flicker component. The power frequency was 50 Hz, derived using a MATLAB toolbox PLL. Gaussian noise was

© 2022 The Author(s). | Published by Institute of Smart Energy Systems Press

introduced to the input signal in the manner described below to gauge the suggested method's effectiveness:

$$Z^k = 1.5\cos(2\pi 50k\tau_s + 80°) \times \left\{1 + \frac{\Delta V_i}{2V_t}\cos(2\pi F_i k\tau_s + \theta_i)\right\} + 0.02 \cdot \text{randn}^k \quad (19)$$

A range of simulations was performed, each injecting a single flicker frequency from **Table 1** into the waveform. The relative voltage amplitude tied to the flicker component, , underwent random selection from the interval [0.001, 0.02]. Moreover, θi values were produced randomly within the [0, 90°] limits. The suggested method computed the relative amplitudes belonging to the flicker components. These final estimated values were compared with the true values, and the absolute error was calculated. Error analysis results from the various simulations are shown in **Figure 2**. While the absolute error tended to increase with increasing amplitude and frequency, the algorithm maintained amplitude estimates within 1% of the true value at all examined frequencies. Convergence patterns were also examined, as shown in **Figure 3**, and delivered acceptable outcomes for every flicker frequency within 0.3 s.

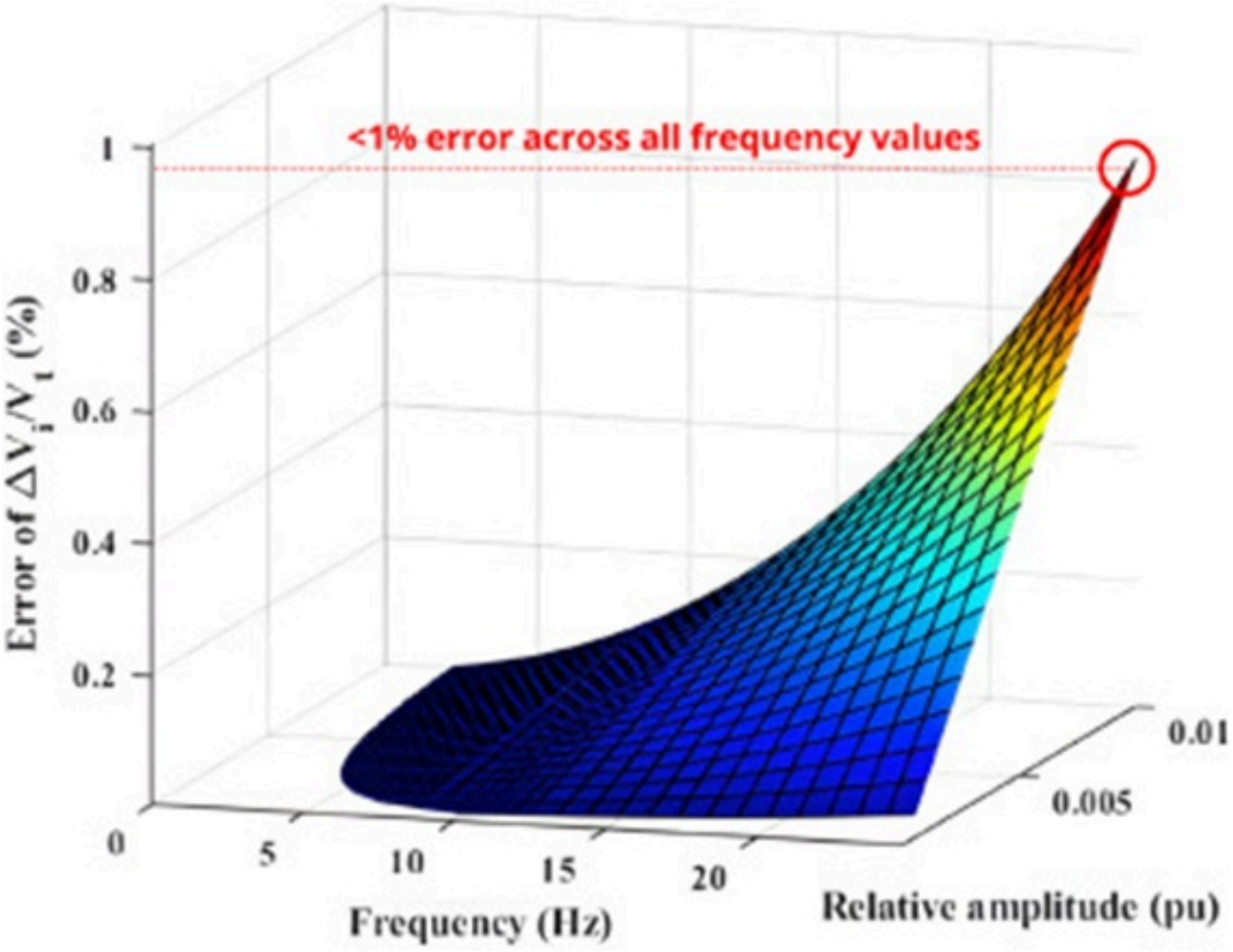

Figure 2. Absolute error of (ΔVi) / Vt estimation, waveform with power frequency and one flicker component.

© 2022 The Author(s). | Published by Institute of Smart Energy Systems Press

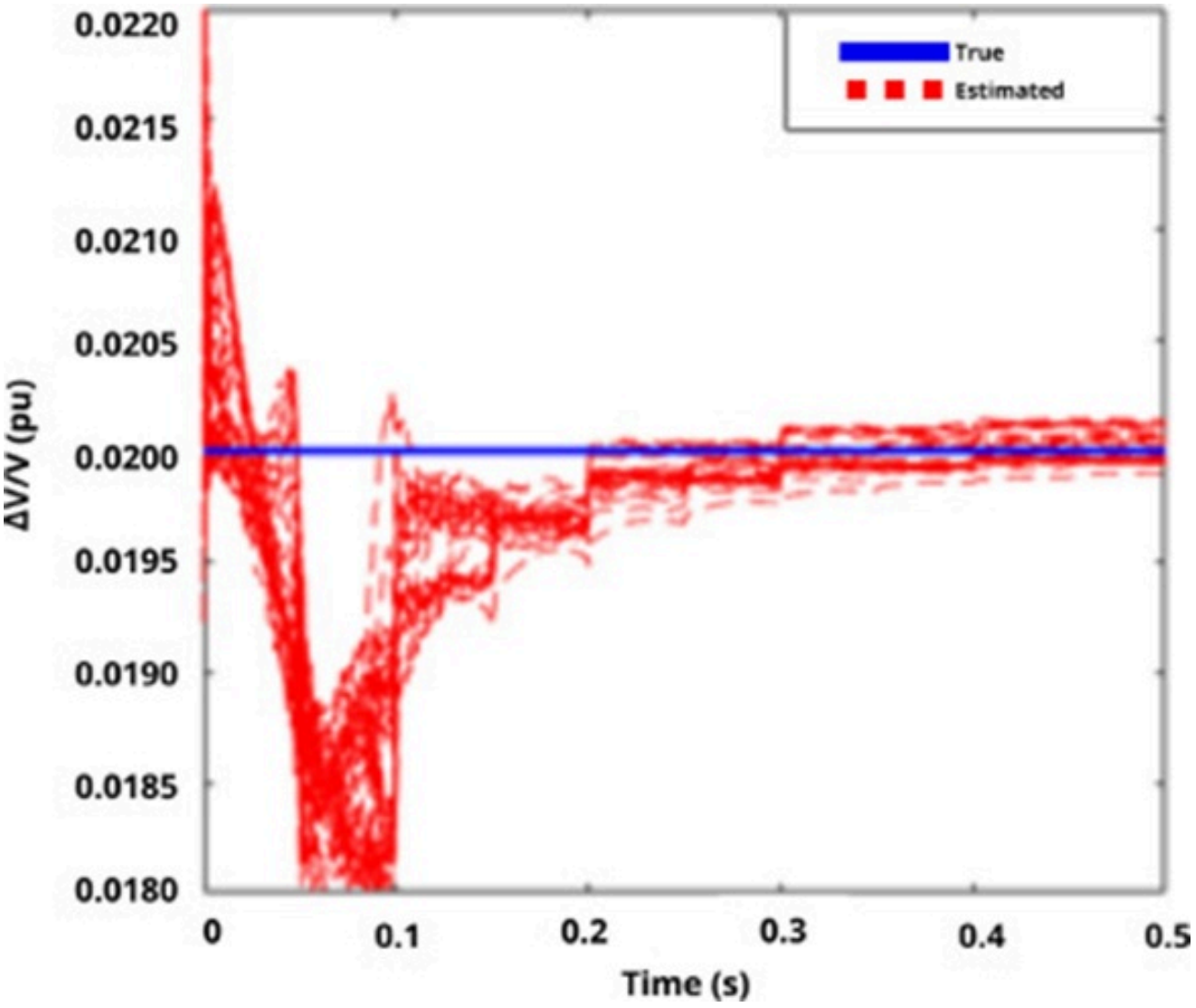

Figure 3. Trend of convergence of the suggested method. The blue line indicates the true relative flicker amplitude $\Delta V / V$ = 0.02 pu. The red lines display the estimated flicker amplitude produced by the ADALINE neural network over time, across several Monte Carlo runs. The plot demonstrates the convergence performance of the estimator for a waveform containing one flicker component.

Estimation of distorted waveform with 5 power harmonics and 36 flicker components

Non-sinusoidal current disturbances along power lines cause real bus voltages to exhibit distorted characteristics, which can be represented as a composite of successive harmonics. This section addresses the flicker estimation challenge using a modulated waveform that contains numerous power harmonics. Furthermore, to test the suggested method across a wide range of flicker frequencies, the fluctuating-voltage waveform was applied at each frequency listed in the IEC 61000-4-15 standard. Consequently, the fluctuating signal from **Eq. 2** takes the following form [19, 23, 47, 48]:

© 2022 The Author(s). | Published by Institute of Smart Energy Systems Press

$$Z^k = \left[1.5\cos\left(2\pi 50k\tau_s + 80°\right) + 0.5\cos\left(2\pi 150k\tau_s + 60°\right) + 0.2\cos\left(2\pi 250k\tau_s + 45°\right) + 0.15\cos\left(2\pi 350k\tau_s + 36°\right) + 0.1\cos\left(2\pi 550k\tau_s + 30°\right)\right] \left\{1 + \sum_{i=1}^{F} \frac{\Delta V_i}{2V_t}\cos\left(2\pi F_i k\tau_s + \theta_i\right)\right\} + 0.02 \cdot \mathrm{randn}^k \quad (20)$$

Table 3 lists the flicker frequencies fi together with their matching amplitudes $\frac{\Delta V_i}{V_t}$. These selected amplitudes were set to achieve unity instantaneous flicker sensation for 230 V/50 Hz systems [38]. At every discrete moment k, the H∞ filter retrieves the signal envelopes. In the studied scenario, five harmonics were present in the simulated signal, requiring the H∞ filter to estimate five separate envelopes. Results for the estimation of the envelope 1 feature in **Figure 4** show that the proposed algorithm converges to the true value within 1 power cycle (0.02 s). The other envelopes followed comparable tracking patterns. Per **Eq. 12**, the H∞ filter also identifies the phases associated with the power harmonic components. Phase estimation results for these harmonics are given in **Figure 5**. The PLL's inaccuracy in pinpointing the exact frequency caused harmonic phase convergence to lag slightly behind envelope convergence.

Nevertheless, convergence of all phases occurred within 0.03 s. Despite these issues, the H-∞ filtering strategy maintained stable outputs owing to its inherent resilience to measurement and modeling uncertainties. Still, refined PLL parameter adjustment or deployment of superior PLL configurations might lessen these impacts.

During the subsequent stage at each time point k, envelopes supplied by the H∞ filter are fed into the ADALINE neural network for determining the flicker components $\frac{\Delta V_i}{V_t}$. **Figure 6** depicts how the ADALINE network tracked flicker amplitudes. Random selection of the network's starting weights led to initial overshoots in the estimates. By handling harmonic and flicker components in isolated stages, the suggested hybrid algorithm enables separate retrieval of parameters across differing magnitudes. This separation reduces the number of iterations needed to reach convergence, finishing processing of the distorted signal in 0.6 s. Reconstructed envelopes, built from the estimated amplitudes, aligned closely with actual values after flicker components stabilized at true levels. **Figure 7** displays the reconstruction accuracy achieved for envelope 1 from the ADALINE outputs, a behavior that extends to the remaining envelopes.

Table 4 compiles the estimation errors observed in the first envelope due to phase-locked loop (PLL) inaccuracies, considering cases with and without fundamental frequency shifts.

Table 3. Flicker frequencies Fi and corresponding relative amplitudes for distorted waveform estimation.

F		*F*		*F*	
0.5	0.0234	6.5	0.003	14	0.00388
1	0.01432	7	0.0028	15	0.00432
1.5	0.0108	7.5	0.00266	16	0.0048
2	0.00882	8	0.00256	17	0.0053
2.5	0.00754	8.8	0.0025	18	0.00584
3	0.00654	9.5	0.00254	19	0.0064
3.5	0.00568	10	0.0026	20	0.007
4	0.005	10.5	0.0027	21	0.0076

© 2022 The Author(s). | Published by Institute of Smart Energy Systems Press

4.5	0.00446	11	0.00282	22	0.00824
5	0.00398	11.5	0.00296	23	0.0089
5.5	0.0036	12	0.00312	24	0.00962
6	0.00328	13	0.00348	25	0.01042

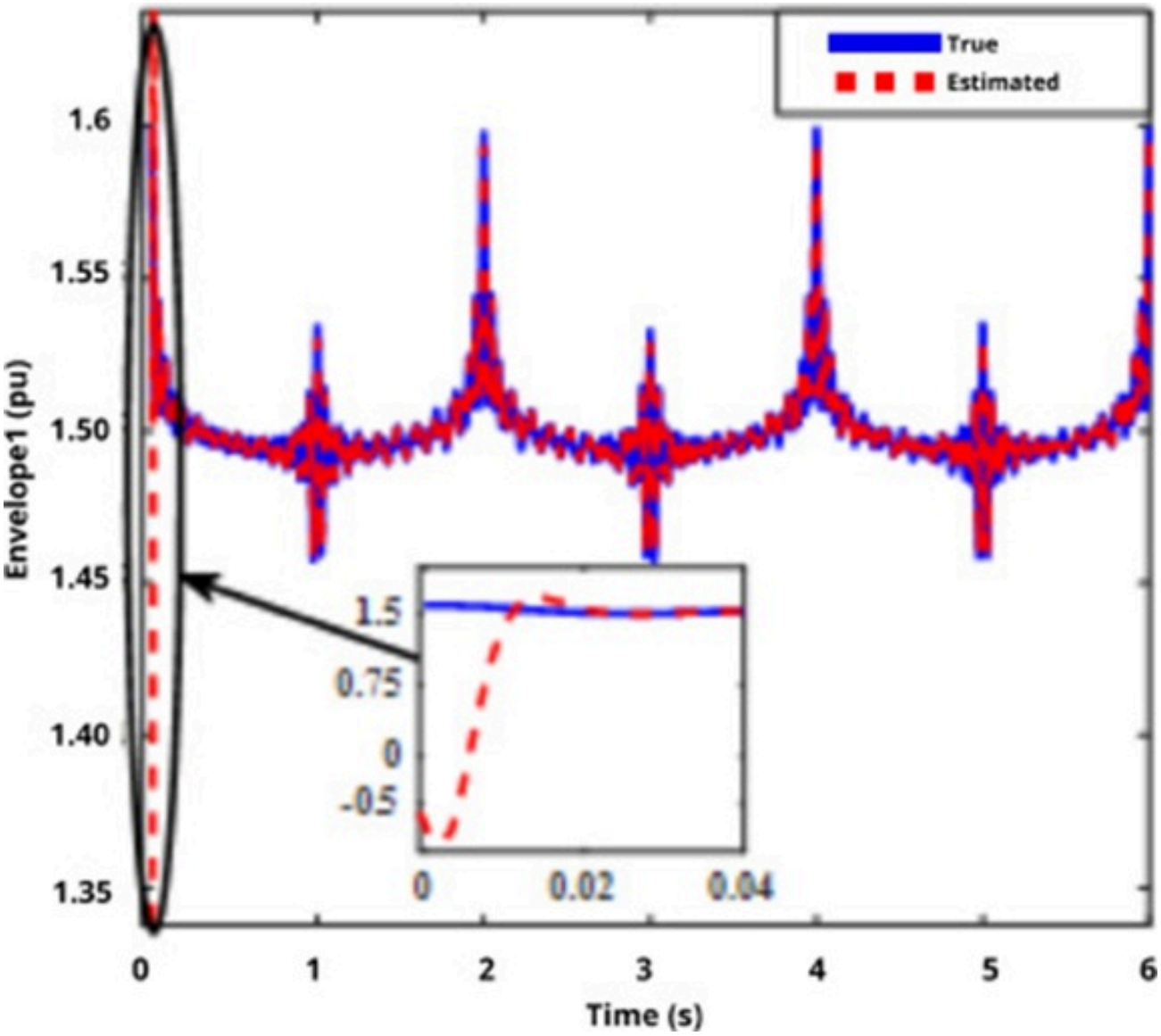

Figure 4. Estimation of envelope 1 using H-infinity filter.

© 2022 The Author(s). | Published by Institute of Smart Energy Systems Press

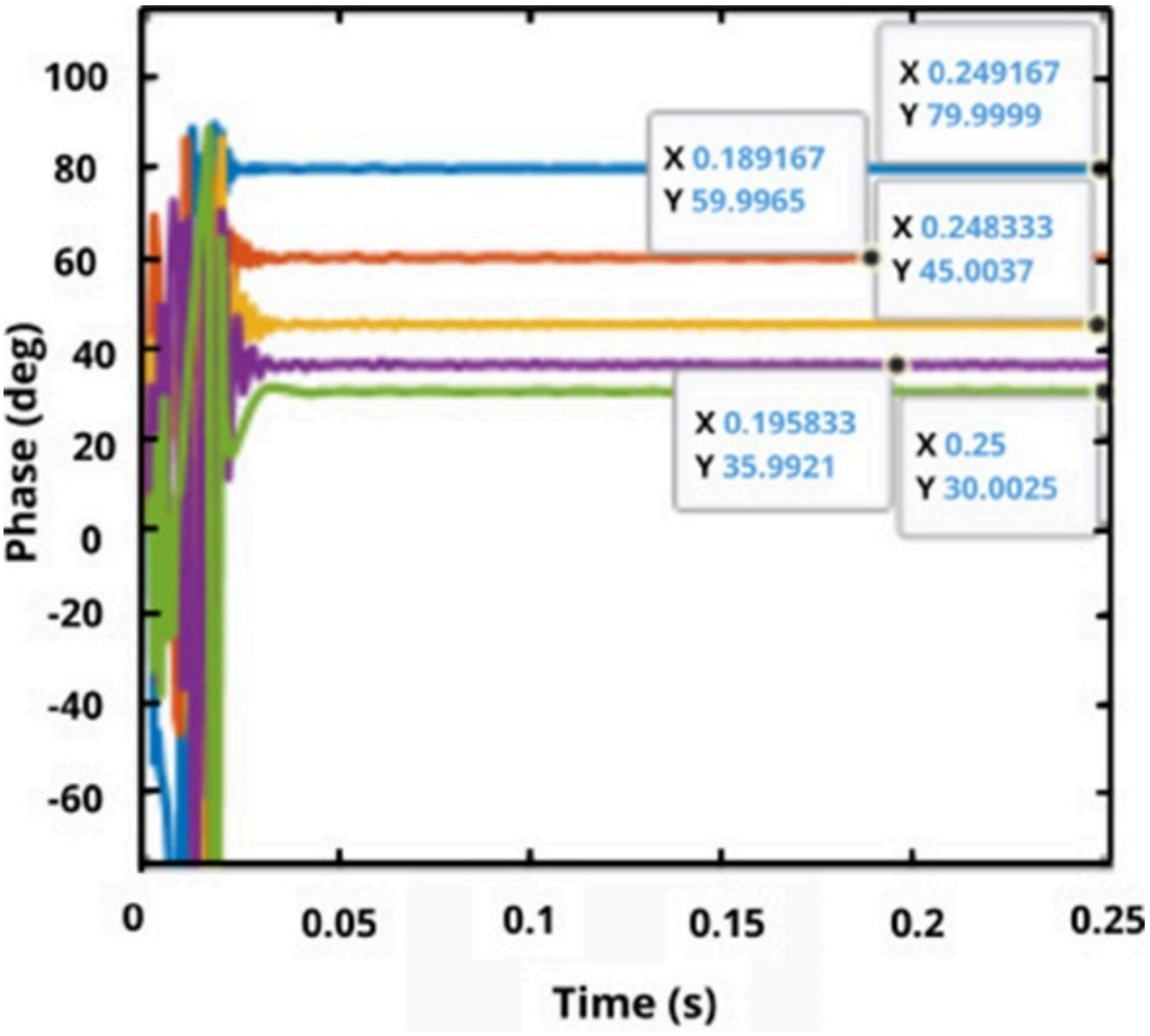

Figure 5. Estimation of power harmonic phases using H-infinity filter. In blue the main components, in red the 3rd component, in orange the 5th component, in purple the 7th component and in green the 11th component.

© 2022 The Author(s). | Published by Institute of Smart Energy Systems Press

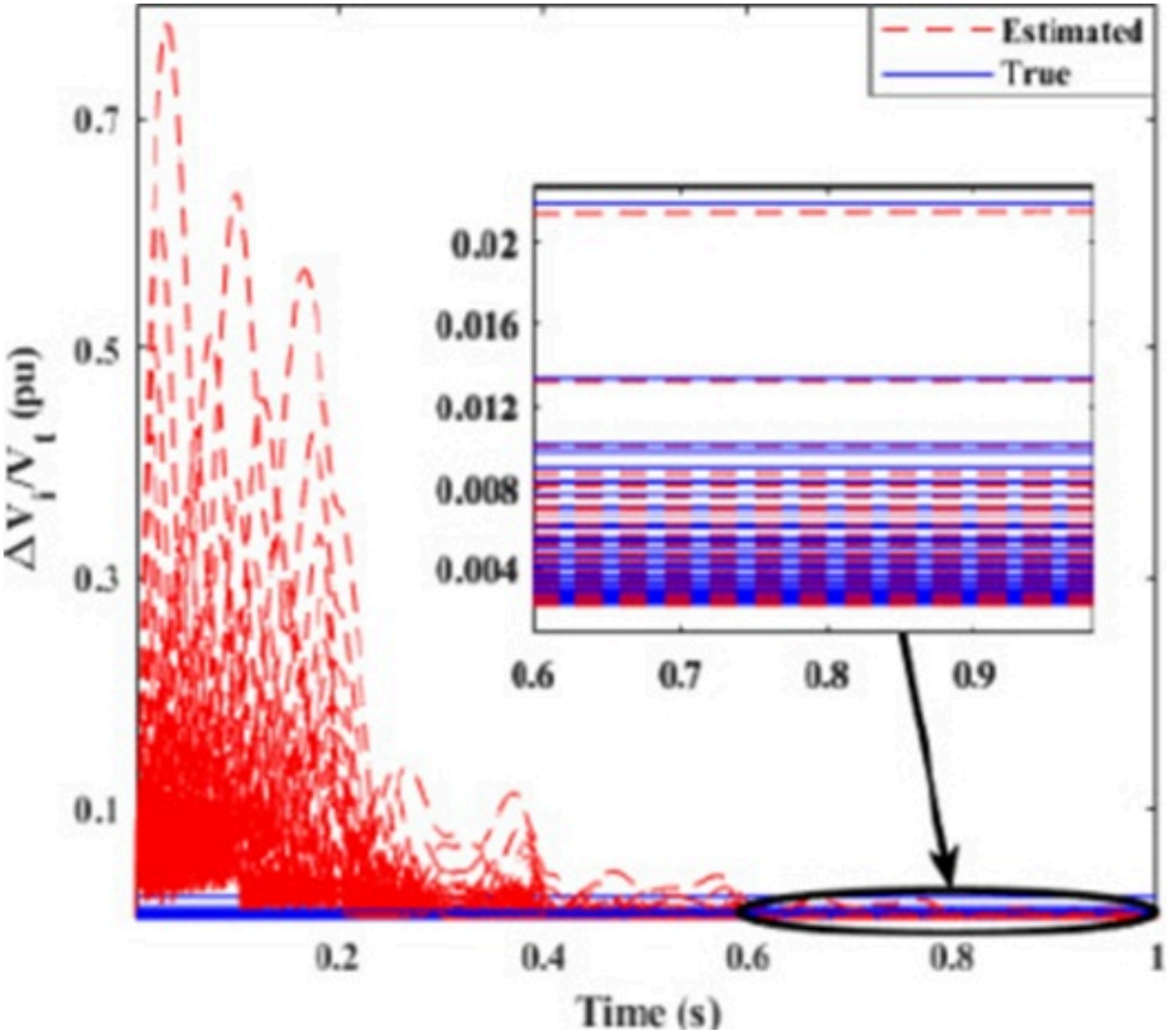

Figure 6. Estimation of flicker amplitudes using ADALINE.

© 2022 The Author(s). | Published by Institute of Smart Energy Systems Press

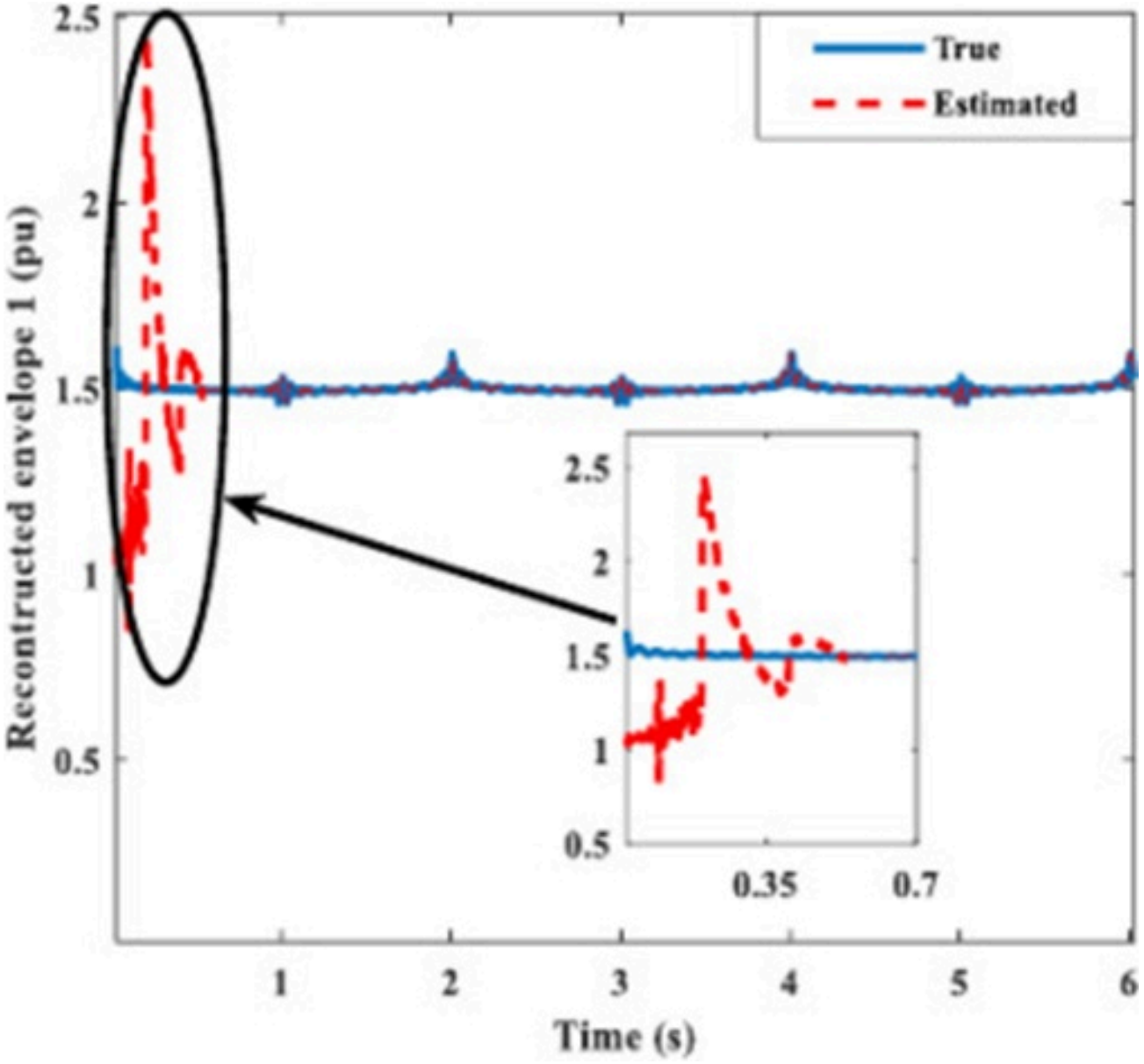

Figure 7. Envelope 1 reconstruction using estimated flicker amplitudes.

According to **Table 4**, the estimation error remained minimal, with no frequency deviations and had a mean of 5.352 and a variance of 4.183. In contrast, a ±0.5 Hz frequency deviation increased both the mean and the variance by more than 10-fold. This outcome emphasizes the vulnerability of PLL-dependent techniques to frequency fluctuations, while highlighting the robustness of the suggested H-∞ filter structure in matching scenarios.

Table 4. Error of envelope 1 estimation due to PLL errors.

Without frequency deviation		With frequency deviation of ±0.5 Hz	
Mean	**Variance**	**Mean**	**Variance**
$5.352e^{-6}$	$4.183e^{-6}$	$7.266e^{-5}$	$8.419e^{-5}$

© 2022 The Author(s). | Published by Institute of Smart Energy Systems Press

Impact of PLL errors and optimization strategies

Table 4 shows that PLL inaccuracies can cause estimation errors, especially during frequency deviation events. Even though the suggested H-∞–ADALINE structure exhibits strong robustness, its overall precision hinges on the PLL's effectiveness in following the fundamental frequency. Adaptive PLL techniques can be introduced to further reduce this contributor to error. Examples include second-order generalized-integrator PLLs (SOGI-PLLs) and adaptive notch-filter PLLs, both of which deliver accelerated convergence and superior performance under changing frequency conditions [49].

Furthermore, careful calibration is required to balance PLL bandwidth and susceptibility to noise, harmonizing tracking accuracy with overall stability. Merging these improved PLL architectures into the suggested method promises greater reliability across varying operating environments and serves as the basis for subsequent investigations.

Monte Carlo (MC) analysis and results discussion

Analyses grounded in MC methods include diverse techniques for problem resolution that rely on random number generation to yield statistical outcomes [6, 19, 50-53]. A key role of MC approaches is to confirm the reliability of estimation algorithms under uncertain conditions. In this research, the MC procedure comprised repeated simulations, each assigning random values to harmonic and flicker amplitudes within the waveform specified by **Eq. 2**. Uniform sampling was used across [0.8, 1.2] for harmonic amplitudes and [0, 0.02] for flicker amplitudes. The suggested estimation procedure then processed these to recover flicker amplitudes. Instantaneous flicker sensation (S), acting as the primary flicker evaluation metric, was derived from the recovered amplitudes to measure estimation fidelity [54, 55]. Each flicker frequency's input to S follows this expression:

$$S_i = \frac{\left(\frac{\Delta V_i}{V_t}\right)}{\left(\frac{\Delta V_i}{V_t}\right)_{\mathrm{IEC}}} \quad (21)$$

Where $\left(\frac{\Delta V_i}{V_t}\right)_{\mathrm{IEC}}$ originates from **Table 3** corresponding to frequency Fi. Overall, estimated S is obtained by aggregating the individual Si contributions. The estimated sensation was compared with the actual sensation, yielding an error percentage as the MC simulation result. **Figure 8** portrays how error in S distributes according to the square root of summed squared harmonic amplitudes $\sqrt{\sum_{n=1}^{N} V_n^2}$ and the square root of summed squared flicker amplitudes $\sqrt{\sum_{i=1}^{F} \left(\frac{\Delta V_i}{V_t}\right)^2}$

Figure 8 indicates that the error in S stayed lower than 0.25% regardless of the random harmonic-flicker amplitude pairings. The convergence characteristics of the algorithm were additionally reviewed across the frequency and time domains via repeated MC executions. A two-dimensional statistical mapping of errors in both S and envelope 1 was conducted in this setting. The outcomes shown in **Figure 9** and summarized in **Table 5** confirm the suggested algorithm's proficiency in capturing the frequency-domain properties of the examined waveform (specifically S values) as well as its accuracy with respect to time-domain aspects (including envelope magnitudes).

© 2022 The Author(s). | Published by Institute of Smart Energy Systems Press

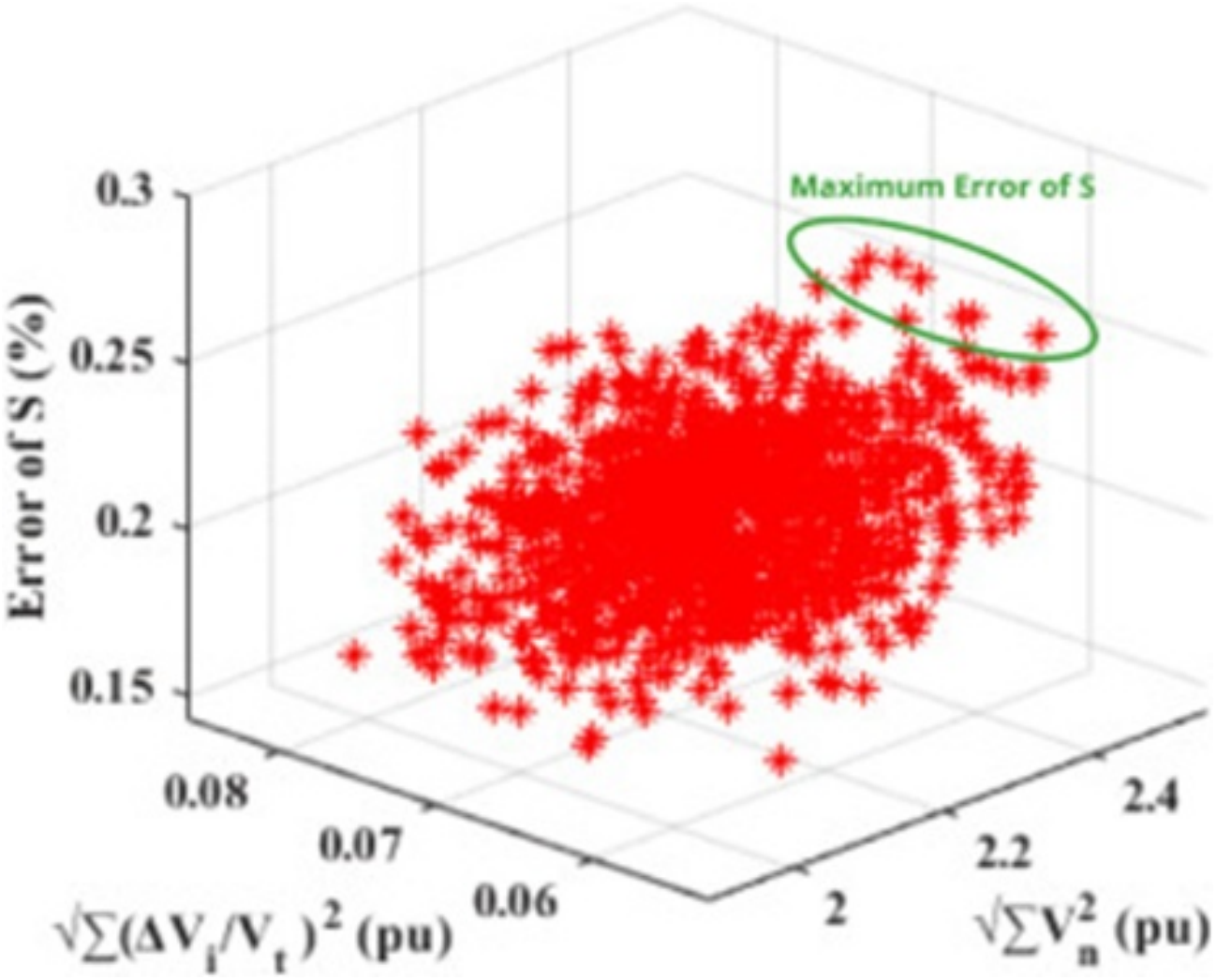

Figure 8. Results of MC analysis for S level estimation.

© 2022 The Author(s). | Published by Institute of Smart Energy Systems Press

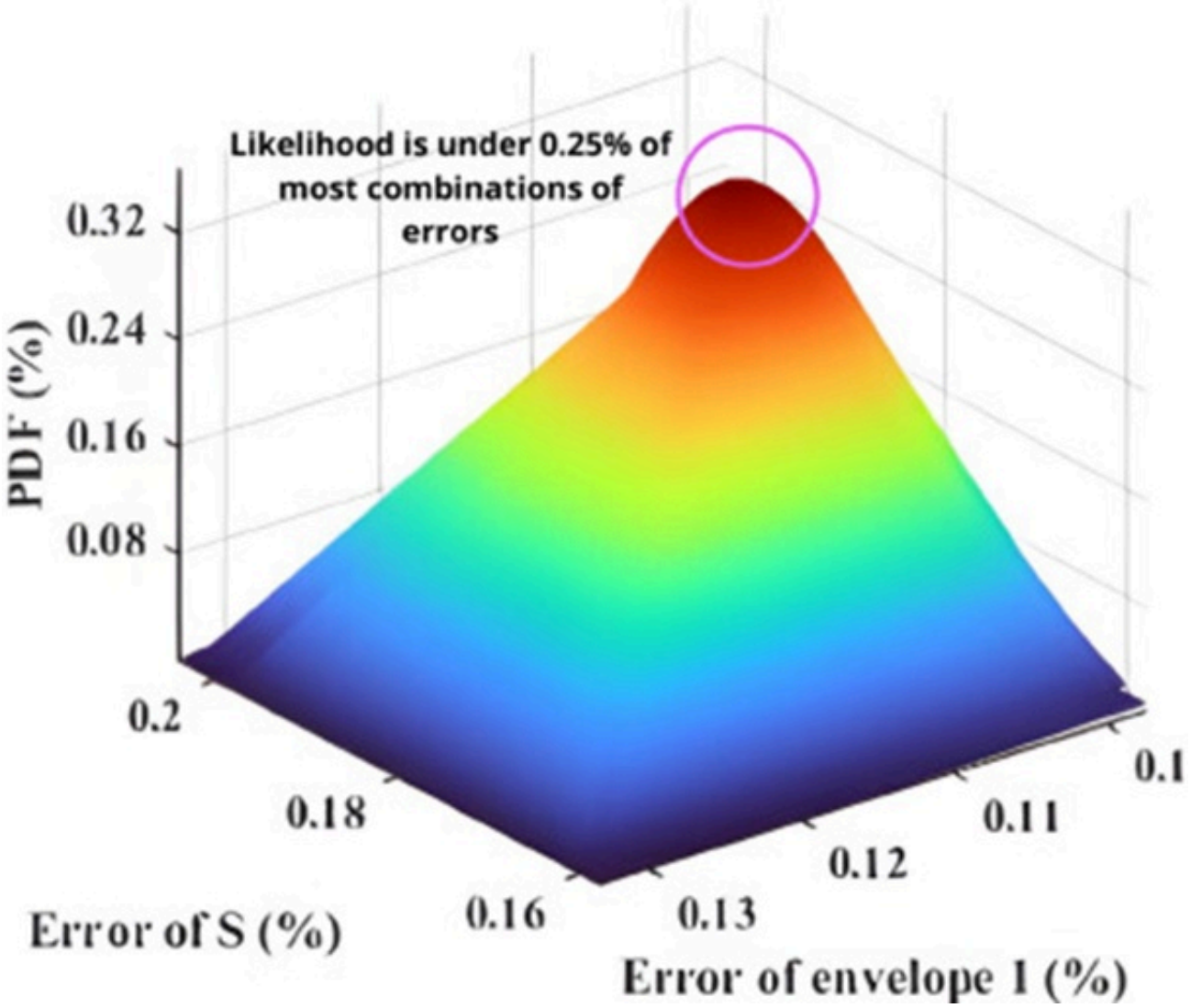

Figure 9. MC statistical analysis for frequency and time domains.

Table 5. Numerical analysis of MC output.

	Error of S (%)	Error of envelope 1 (%)
Mean	0.1832	0.1114
STD[a]	0.0021	0.0038

[a] Standard deviation

Theoretical and practical insights

Simulation experiments had already confirmed the theoretical capabilities of the suggested technique. This section explores the algorithm's suitability for actual field conditions. In addition, the standard Fast Fourier Transform (FFT) and the modern Discrete Wavelet Transform (DWT) approaches from MATLAB toolboxes were employed to estimate flicker components under matching test setups, and direct comparisons were made. A laboratory configuration was built to record genuine data from a varying voltage supply. The voltage signal originates from a 400 V infinite bus that feeds die-

© 2022 The Author(s). | Published by Institute of Smart Energy Systems Press

casting machines with capacities ranging from 160 to 1000 tons, electrostatic painting units, and oil pumps at Mazinoor Lighting Industries Inc. Rapid load shifts in the die-casting machines trigger sharp current swings, which, in turn, produce variations in the supply voltage. These machines were chosen for their frequent and intense transients, clearly demonstrating the durability and real-time operation of the proposed technique. To illustrate broader use, additional evaluations involving inverter-fed loads, such as variable-frequency drives (VFDs) or induction motors — frequent sources of harmonics and flicker in factory settings — are suggested for future research. Machine input voltage was measured using a quick-response voltage transducer (LV 25-P), and data were acquired with an NI USB-6009 DAQ card at a 1200 Hz sampling rate over 6 s. The test arrangement is illustrated in **Figure 10a**, and the data-acquisition layout is shown in **Figure 10b.** The acquired data was analyzed offline in MATLAB using the suggested algorithm, along with FFT and DWT techniques. Processing was performed on a computer with a Core i5 processor running at 3.1 GHz and 8 GB of RAM. **Figure 11** shows plotted outcomes for envelope 1 obtained from the three techniques. Sudden load variations produced prominent notches in the measured signal, yet the estimated envelope 1 closely followed the actual envelope trajectory. For closer inspection, the low-voltage segment of the test signal was enlarged, demonstrating stronger results from the suggested algorithm and DWT technique than from FFT in both constant and dynamic states. The rebuilt signal, created using the computed flicker components and harmonic values, was matched to the recorded signal. Error measures for the final two seconds (4 s to 6 s) of recorded data across FFT, DWT, and the suggested techniques are summarized in **Table 6.** Although visual plots appeared promising, quantitative indicators showed that the DWT technique achieved lower precision in real environments. The chief factor behind this reduced performance in the DWT time-frequency technique is the presence of high-frequency noise in the field data, which leads to aliasing.

In the following test, the main feeder was switched off, and the load was supplied through a diesel emergency generator. Live recordings revealed frequency shifts of ±0.25 Hz during die-casting machine activity. Under these circumstances, PLL outputs for fundamental frequency tracking are distorted by interference (noise or narrowband signals), thereby affecting the precision of the suggested technique. Although accuracy declined across all techniques in this scenario, the suggested technique remained stable by separating voltage fluctuations from harmonic components, thereby reducing the influence of frequency disturbances. As a result, PLL error contributions were lessened in the produced outputs. Nonetheless, the combination of aliasing and picket-fence phenomena lowered the effectiveness of FFT and DWT techniques. Numerical findings are listed in **Table 6**, including an evaluation of processing demands for the three techniques over the last two seconds of data. The suggested technique delivered the strongest processing efficiency under standard conditions (stable feeder). However, during frequency shifts, processing time increased modestly beyond that of the FFT technique due to the need for additional iterations to achieve satisfactory results. Despite delivering accurate results, the DWT technique imposes a heavy computational burden, limiting its practicality for real-time applications. Values presented in **Table 6** emphasize the suggested hybrid technique's capacity to achieve both precise and streamlined estimation of flicker components in real-world use.

Although the present research mainly addresses flicker estimation, the hybrid technique's flexible framework — integrating H-∞ filtering with ADALINE networks — can be modified to address other power quality issues, such as voltage sags, swells, and interharmonics. Subsequent studies should directly validate this broader application, possibly modifying the model structure to incorporate additional frequency and amplitude changes typical of these issues.

© 2022 The Author(s). | Published by Institute of Smart Energy Systems Press

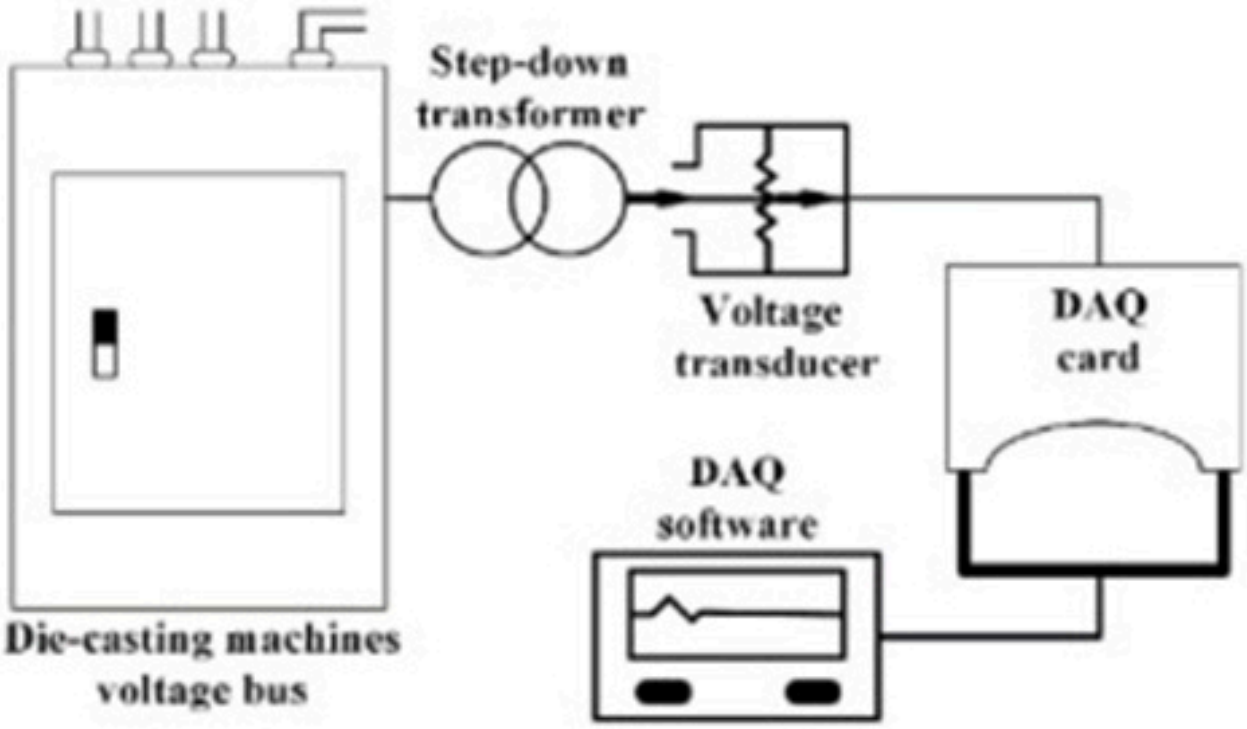

(a) Testbench schematic

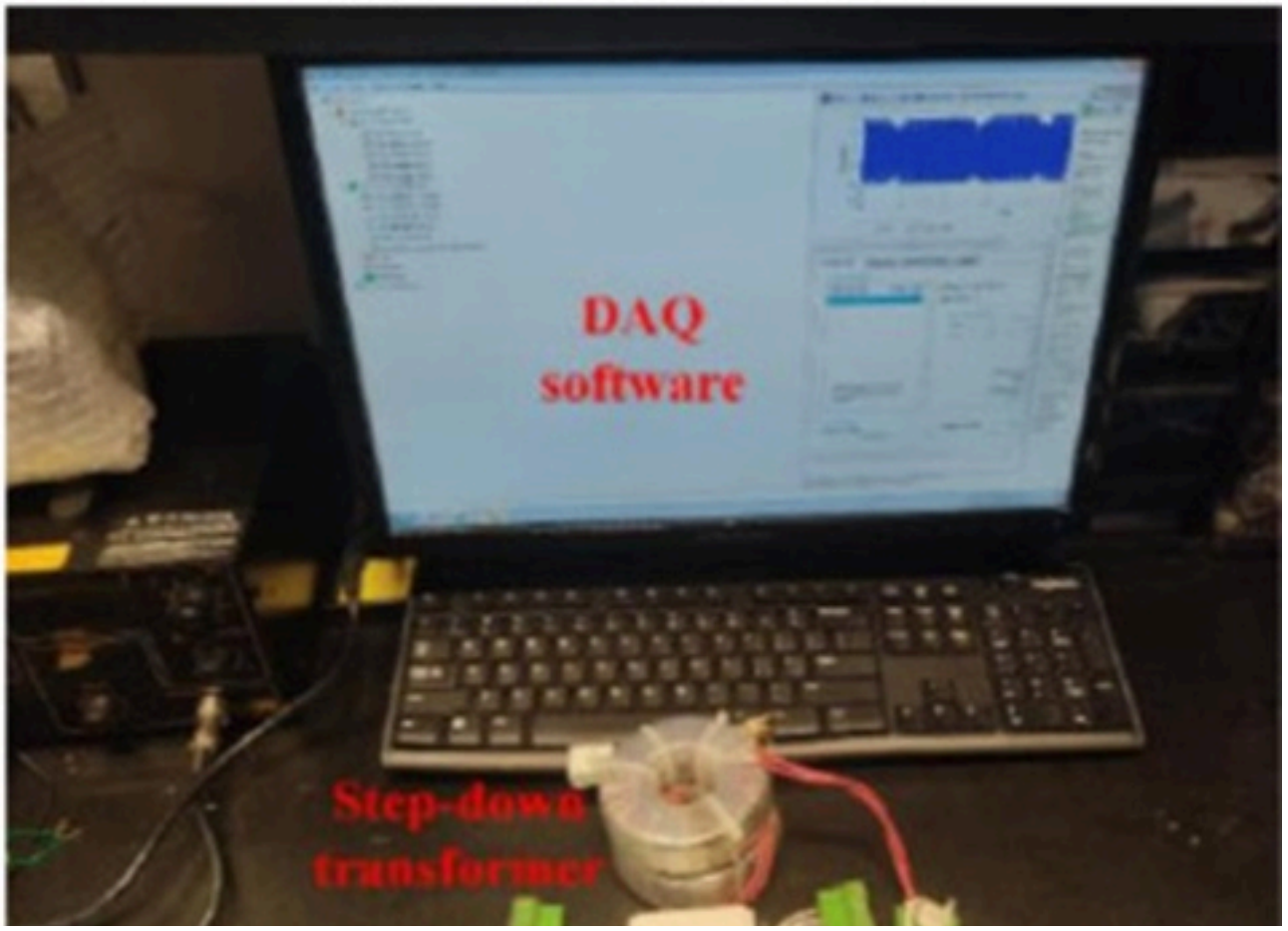

© 2022 The Author(s). | Published by Institute of Smart Energy Systems Press

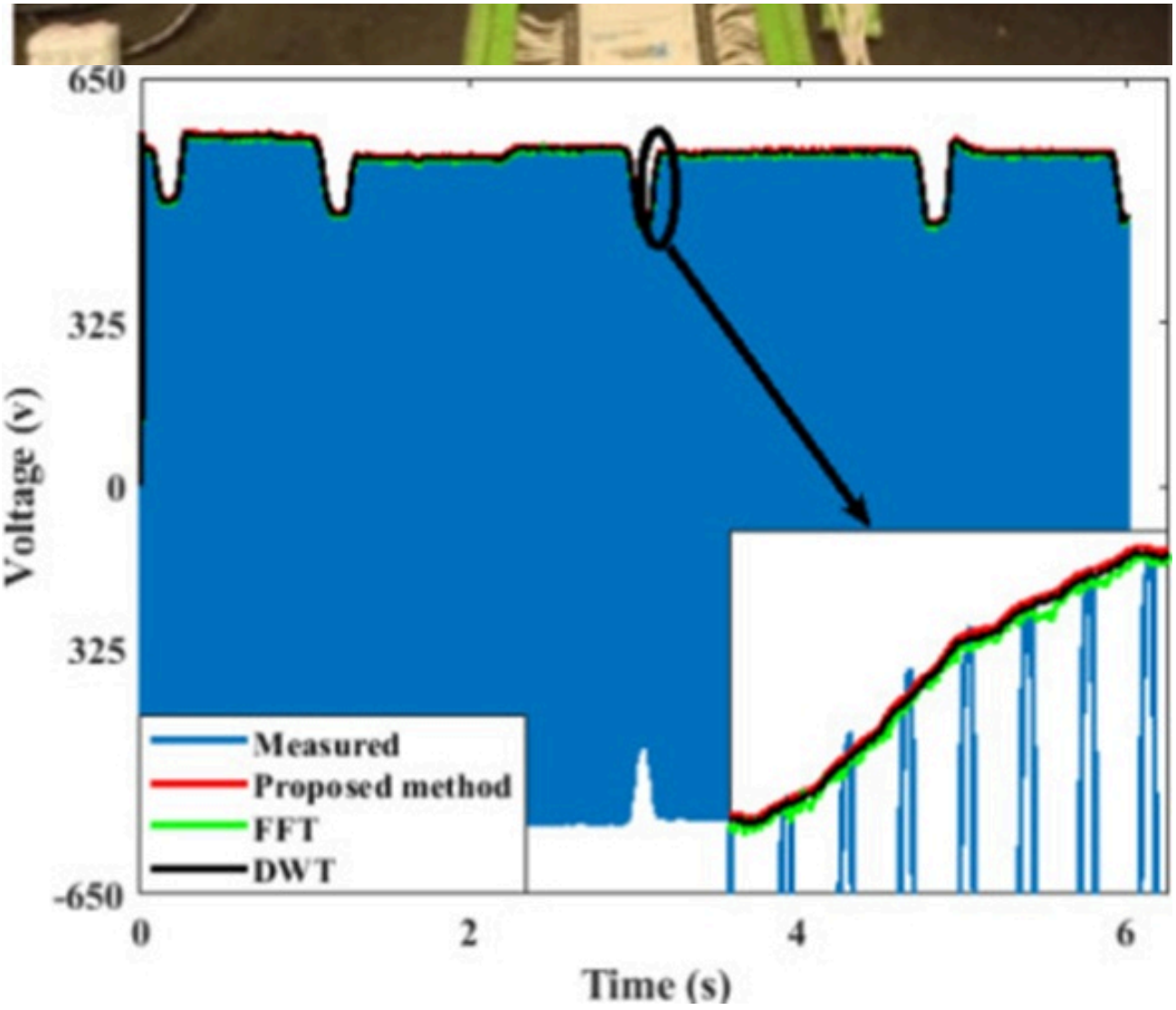

Figure 11. Experimental signal analysis using different methods for validation.

Table 6. Numerical analysis of practical data.

Method	Feature	MSE	Variance	Computational time
	Proposed method	$7.776e^{-6}$	$5.911e^{-6}$	0.3812 s
Infinite feeder	FFT	$4.367e^{-5}$	$1.019e^{-4}$	0.4182 s
	DWT	$7.8115e^{-6}$	$7.381e^{-5}$	0.8338 s
	Proposed method	$1.912e^{-4}$	$4.54e^{-4}$	0.4290 s
Emergency diesel	FFT	$3.007e^{-3}$	$5.672e^{-4}$	0.4194 s
	DWT	$2.716e^{-4}$	$4.705e^{-4}$	0.8627 s

© 2022 The Author(s). | Published by Institute of Smart Energy Systems Press

Parameter selection and optimization

The effectiveness of the suggested H-∞–ADALINE technique depends on several critical parameters. For the H-∞ filter, the weighting matrices and the regularization factor λ were determined to achieve a balance between resilience to measurement noise and stability assurance, consistent with conventional design guidelines. Adopted values ensure bounded estimation error while supporting quick reaction during varying disturbances.

Regarding the ADALINE network, the initial learning rate θ0 and decay factor β **(Eq. 17)** were adjusted using sensitivity studies. Increased θ0 values accelerate convergence but raise instability risks, whereas reduced values strengthen stability at the expense of slower adaptation. In this work, the selected parameters offered a balanced compromise, as verified through Monte Carlo simulations under IEC 61000-4-15 test conditions.

Although manual adjustment delivered acceptable outcomes, structured optimization techniques, such as Bayesian optimization, genetic algorithms, or adaptive gain scheduling, could further improve parameter durability, especially in large or rapidly changing systems. The integration of such automatic tuning approaches will be a focus of future research.

Scalability and feasibility considerations

Although the suggested hybrid H-∞–ADALINE strategy was validated within the IEC-specified flicker frequency interval (0.5–25 Hz), its efficient recursive design indicates strong potential for expansion to larger distribution networks. The H-∞ filter performs only matrix updates per iteration, and the ADALINE network employs a single-layer structure that does not require offline training, rendering both suitable for live deployment in power quality monitoring equipment.

However, extensive interconnected power networks pose additional challenges, including intricate harmonic couplings, interharmonics, and unsynchronized disturbances, which may reduce estimation precision. Moreover, broadening the examination beyond the 25 Hz limit (for instance, into the supraharmonic range) could necessitate alterations to ADALINE basis functions or incorporation of multi-resolution techniques to detect higher-frequency behaviors.

Hence, while the suggested technique appears conceptually appropriate for scaling to large systems and high-frequency ranges, future efforts will prioritize practical confirmation through field measurements and algorithm refinements to improve robustness in complex grid environments.

Conclusion

This article proposes an innovative algorithm for estimating flicker frequency components in voltage waveforms, addressing the intrinsic challenges posed by the broad range of frequencies present. The suggested technique successfully separates the voltage waveform into envelope and harmonic elements, considerably simplifying the estimation procedure. Envelopes are precisely obtained via a resilient H-∞ filter, after which an online ADALINE neural network rapidly identifies the flicker content inside those envelopes. Furthermore, the research introduces a new voltage waveform model that includes flicker, harmonics, and white noise to fully evaluate the algorithm’s effectiveness.

Visual and quantitative outcomes verify the effectiveness of the proposed technique in precisely monitoring power system flicker. Monte Carlo simulations additionally validate its durability across various harmonic and flicker situations consistent with IEC Standard 61000-4-15. Real-world relevance was confirmed through actual voltage fluctuation recordings, showing that the proposed technique outperforms conventional FFT and DWT methods in terms of Mean Square Error (MSE), variance, and processing efficiency.

Primary advantages of this technique include strong resistance to measurement noise, swift convergence appropriate for live use, and computational efficiency suitable for hardware-limited settings. Taken together, these qualities position the proposed technique as highly appropriate for industrial power-quality monitoring.

© 2022 The Author(s). | Published by Institute of Smart Energy Systems Press

Even with these benefits, the technique has some constraints. The fixed-frequency grid, while aligned with standards, might reduce precision for frequencies outside the grid. Moreover, testing focused mainly on die-casting machine loads, limiting its applicability to other industrial contexts. The lack of representation for contemporary lighting systems, particularly LEDs, constitutes an additional limitation.

Future investigations might examine effects from higher-order harmonics, flickers, and interharmonics. Evaluation of other robust online neural networks, such as Online Recurrent Neural Networks (RNNs) or Echo State Networks, could improve prediction precision and processing speed. In addition, developing a model that accurately captures the flicker characteristics of modern LED lighting systems offers a significant avenue for ongoing research.

Acknowledgements

None

Conflict of interest

None

Financial support

The authors declare the following financial interests/personal relationships which may be considered as potential competing interests: Pedram Asef reports financial support was provided by University College London. If there are other authors, they declare that they have no known competing financial interests or personal relationships that could have appeared to influence the work reported in this paper.

Ethics statement

None

Received: 19 Jul 2021 Revised: 23 Sep 2021 Accepted: 08 Oct 2021
Published online: 15 June 2022

Rights and permissions

Open Access The author(s) retain copyright. This article is licensed under the Creative Commons Attribution-NonCommercial-ShareAlike 4.0 International License. It may be shared and adapted for non-commercial purposes with appropriate attribution, an indication of changes, and distribution of adaptations under the same license. Third-party material may be subject to separate terms identified in its credit line. View the license at https://creativecommons.org/licenses/by-nc-sa/4.0/.

References

1. IEEE Application Guide for IEEE Standard for Interconnecting Distributed Resources with Electric Power Systems. IEEE Std. 1547.2-2008. 2008.

2. Kuwalek P. Estimation of parameters associated with individual sources of voltage fluctuations. IEEE Trans Power Deliv. 2015;36:351-61.

3. Farhan M, Reza TN, Badal FR, Islam MR, Muyeen SM, Tasneem Z, et al. Towards next generation internet of energy system: Framework and trends. Energy AI. 2023;14:100306.

4. Mitchell D, Blanche J, Harper S, Lim T, Gupta R, Zaki O, et al. A review: Challenges and opportunities for artificial intelligence and robotics in the offshore wind sector. Energy AI. 2022;8:100146.

5. Bucci G, Fiorucci E, Ciancetta F. The performance evaluation of IEC flicker meters in realistic conditions. IEEE Trans Instrum Meas. 2008;57:2443-9.

6. Kukačka L, Dupuis P, Vik M, Richter A, Zissis G. Confidence intervals for luminous flicker measurements: Comparison of various approaches. IEEE Trans Ind Appl. 2021;57:5499-506.

7. IEC. Electromagnetic compatibility (EMC)—part 4-15 testing and measurement techniques—flickermeter—functional and design specifications. IEC Std. 61000-4-15. 2010:1-58.

8. Wiczyński G. Estimation of pst indicator values on the basis of voltage fluctuation indices. IEEE Trans Instrum Meas. 2017;66:2046-55.

9. IEC Report: Flickermeter. Functional and Design Specifications. IEC 80 868-0. 1986.

10. Li F, Ye M. Calculation of Flicker Parameters Using Voltage Interharmonics. In: 2012 Asia-Pacific Power and Energy Engineering Conference (APPEEC). Shanghai, China; 2012. p. 1-4.

11. Zakaria D, Sunarno E, Anggriawan DO, Putra Ganda W. Real Time Voltage Flicker Detection Based on Fast Fourier Transform. In: 2019 International Electronics Symposium (IES). Surabaya, Indonesia; 2019. p. 164-9.

12. Li Y, Gao Y, Feng Y, Cao Y, Zhu Y. Improved analytic energy operator and novel three-spectral line interpolation DFT method for parameter estimation of voltage flicker. IEEE Trans Ind Inform. 2024;20(1):327-36.

13. Chen MT. Digital algorithms for measurement of voltage flicker. IEE Proc Gener Transm Distrib. 1997;144:175-80.

14. Marei MI, El-Saadany EF, Salama MMA. Estimation techniques for voltage flicker envelope tracking. Electr Power Syst Res. 2004;70:30-7.

15. Abdel-Galil TK, El-Saadany EF, Salama MMA. Online tracking of voltage flicker utilizing energy operator and Hilbert transform. IEEE Trans Power Deliv. 2004;19:861-7.

16. Darvish Falehi A, Rafiee M. LVRT/HVRT capability enhancement of DFIG wind turbine using optimal design and control of novel PI d-AMLI based DVR. Sustain Energy Grids Netw. 2018;16:111-25.

17. Li F, Gao Y, Cao Y, Iravani R. Improved teager energy operator and improved chirp-z transform for parameter estimation of voltage flicker. IEEE Trans Power Deliv. 2016;31:245-53.

18. Yao W, Tang Q, Teng Z, Gao Y, Wen H. Fast S-transform for time-varying voltage flicker analysis. IEEE Trans Instrum Meas. 2014;63:72-9.

19. Enayati J, Moravej Z. Real-time harmonic estimation using a novel hybrid technique for embedded system implementation. Int Trans Electr Energy Syst. 2017;27:1-13.

20. Sun J, Aboutanios E, Smith DB, Fletcher JE. Robust frequency, phase, and amplitude estimation in power systems considering harmonics. IEEE Trans Power Deliv. 2020;35:1158-68.

© 2022 The Author(s). | Published by Institute of Smart Energy Systems Press

21. Duda K, Zieliński TP, Bień A, Barczentewicz SH. Harmonic phasor estimation with flat-top FIR filter. IEEE Trans Instrum Meas. 2020;69:2039-47.

22. Dai Z, Lin W. Adaptive estimation of three-phase grid voltage parameters under unbalanced faults and harmonic disturbances. IEEE Trans Power Electron. 2017;32:5613-27.

23. Enayati J, Moravej Z. Real-time harmonics estimation in power systems using a novel hybrid algorithm. IET Gener Transm Distrib. 2017;11:3532-8.

24. Garanayak P, Naayagi RT, Panda G. A high-speed master-slave ADALINE for accurate power system harmonic and inter-harmonic estimation. IEEE Access. 2020;8:51918-32.

25. Saleh SA. Phaselet transform based approach for detecting voltage flickers due to distributed generation units. IEEE Trans Ind Appl. 2018;54:5278-92.

26. Saleh SA. The extended Newton–phaselet method for determining the reactive power from the active power in single–phase systems. IEEE Trans Ind Appl. 2016;52:1297-307.

27. Sun D, Gao Q, Lu Y, Zhu M. A sparse representation-based algorithm for the voltage fluctuation detection of power system. Digit Signal Process. 2016;48:259-68.

28. Kuwalek P. AM modulation signal estimation allowing further research on sources of voltage fluctuations. IEEE Trans Ind Electron. 2020;67:6937-45.

29. Yang X, Kratz X. Power system flicker analysis by RMS voltage values and numeric flicker meter emulation. IEEE Trans Power Deliv. 2009;24:1310-8.

30. Geiger DL, Halpin SM. Assessing voltage fluctuations and lamp flicker using RMS voltages. IEEE Trans Power Deliv. 2017;32:2481-8.

31. Balouji E, Salor O. Digital realisation of the IEC flickermeter using root mean square of the voltage waveform. IET Gener Transm Distrib. 2016;10:1663-70.

32. Cho SH, Park CH, Han J, Jang G. A waveform distortion evaluation method based on a simple half-cycle RMS calculation. IEEE Trans Power Deliv. 2012;27:1461-7.

33. Eghtedarpour N, Farjah E, Khayatian A. Intelligent identification of flicker source in distribution systems. IET Gener Transm Distrib. 2010;4:1016-27.

34. Moghadam BH, Abbasi M, Tousi B. A new method with minimum number of monitoring points for flicker source tracing by wavelet transform. Int Trans Electr Energy Syst. 2019;29.

35. Samet H, Khosravi M, Ghanbari T, Tajdinian M. A two-level neural network approach for flicker source location. Comput Electr Eng. 2021;92.

36. Kose N, Salor O, Leblebicioglu K. Kalman filtering based approach for light flicker evaluation of power systems. IET Gener Transm Distrib. 2011;5:57-69.

37. Al-Hamadi HM. Fuzzy logic voltage flicker estimation using Kalman filter. Electr Power Energy Syst. 2012;36:60-7.

38. Salor N, Leblebicioglu O, Leblebicioglu K. Interharmonics analysis of power signals with fundamental frequency deviation using Kalman filtering. Electr Power Syst Res. 2010;80:1145-53.

© 2022 The Author(s). | Published by Institute of Smart Energy Systems Press

39. Pramanik M, Routray A, Mitra P. A two-stage adaptive symmetric-strong-tracking square-root cubature Kalman filter for harmonics and interharmonics estimation. Electr Power Syst Res. 2022;210:108133.

40. Enayati J, Asef P, Yousefi A, Benoit A. A novel AI-driven hybrid method for flicker estimation in power systems. In: 7th International Conference on Smart Energy Systems and Technologies (SEST). Torino, Italy; 2024.

41. Li W, Jia Y. H-infinity filtering for a class of nonlinear discrete-time systems based on unscented transform. Signal Process. 2010;90(12):3301-7.

42. Marei MI, El-Saadany EF, Salama MMA. An intelligent control for the DG interface to mitigate voltage flicker. In: Eighteenth Annual IEEE Applied Power Electronics Conference and Exposition (APEC '03). Vol. 1. Miami Beach, FL, USA; 2003. p. 179-83.

43. Sujith M, Padma S. Optimization of harmonics with active power filter based on ADALINE neural network. Microprocess Microsyst. 2020;73:102976.

44. Peng Z, Goh R, Mohd M, Hizam H, Wahab A, Izzri N. A simple predictive method of critical Flicker detection for human healthy precaution. Math Probl Eng. 2015;871826:10.

45. Dash PK, Swain DP, Routry A, Liew AC. Harmonic estimation in a power system using adaptive perceptrons. IEE Proc Gener Transm Distrib. 1996;143:565-74.

46. Simon D. Optimal State Estimation: Kalman, H Infinity, and Nonlinear Approaches. Hoboken, NJ, USA: Wiley; 2006.

47. Carbajala FB, Olverab RT. An adaptive neural online estimation approach of harmonic components. Electr Power Syst Res. 2020;186:106406.

48. Moravej Z, Enayati J. A hybrid least squares-clonal selection based algorithm for harmonic estimation. Int Trans Electr Energy Syst. 2014;12:1-15.

49. Xu J, Qian H, Hu Y, Bian S, Xie S. Overview of SOGI-based single-phase phase-locked loops for grid synchronization under complex grid conditions. IEEE Access. 2021;9:39275-91.

50. Enayati J, Rahimnejad A, Gadsden SA. LED reliability assessment using a novel Monte Carlo-based algorithm. IEEE Trans Device Mater Reliab. 2021;21:338-47.

51. Enayati J, Sarhadi P, Rad MP, Zarini M. Monte Carlo simulation method for behavior analysis of an autonomous underwater vehicle. J Eng Marit Environ. 2015;230:481-90.

52. Matthews C, Clarkson P, Harris PM, Ihlenfeld WGK, Wright PS. Evaluation of Flicker measurement uncertainties by a Monte Carlo method. IEEE Trans Instrum Meas. 2011;60:2255-61.

53. Almeida FS, Silveira FH, Visacro S. Stopping criterion for Monte Carlo method-based simulations of the lightning performance of transmission line. Electr Power Syst Res. 2023;214:108797.

54. Ferrero A, Salicone S, Toscani S. A fast, simplified frequency-domain interpolation method for the evaluation of the frequency and amplitude of spectral components. IEEE Trans Instrum Meas. 2011;60(5):1579-87.

55. Xu Y, Yi H, Zhang W, Xu H. An improved CZT algorithm for high-precision frequency estimation. Appl Sci. 2023;13:1907.

© 2022 The Author(s). | Published by Institute of Smart Energy Systems Press